BMC Genomics

RESEARCH Open Access

Combined metabolome and transcriptome analysis reveal the mechanism of water stress in *Ophiocordyceps sinensis*

Li He[1], ChuanYong Li[1], ZhaoHe Chen[1], YanLi Huo[1], Bo Zhou[1] and Fang Xie[1*]

Abstract

Background *Ophiocordyceps sinensis* (*O. sinensis*) is the dominant bacterium in the asexual stage of *Chinese cordyceps*, and its growth usually suffers from water stress. Thus, simulating its ecological growth environment is crucial for artificial cultivation. This study aimed to reveal the mechanism underlying the water stress tolerance of *Ophiocordyceps sinensis* (*O. sinensis*) by combining metabolomic and transcriptome analyses to identify crucial pathways related to differentially expressed genes (DEGs) and metabolites (DEMs) involved in the response to water stress.

Results Gene coexpression analysis revealed that many genes related to 'betalain biosynthesis', 'tyrosine metabolism', 'linoleic acid metabolism', 'fructose and mannose metabolism', and 'starch and sucrose metabolism' were highly upregulated after 20d-water stress. Metabolomic analysis revealed that many metabolites regulated by these genes in these metabolic pathways were markedly decreased. On the one hand, we surmised that carbohydrate metabolism and the β-oxidation pathway worked cooperatively to generate enough acyl-CoA and then entered the TCA cycle to provide energy when exposed to water stress. On the other hand, the betalain biosynthesis and tyrosine metabolism pathway might play crucial roles in response to water stress in *O. sinensis* by enhancing cell osmotic potential and producing osmoregulatory substances (betaine) and antioxidant pigments (eumelanin).

Conclusions Overall, our findings provide important information for further exploration of the mechanism underlying the water stress tolerance of *O. sinensis* for the industrialization of artificial cultivation of *Chinese cordyceps*.

Keywords *Ophiocordyceps Sinensis*, Water stress, RNA-seq, WGCNA, Metabolites

*Correspondence:
Fang Xie
xfrankf@163.com
[1]School of Biological and Pharmaceutical Engineering, Lanzhou Jiaotong University, Lanzhou, Gansu, P. R. China

Background

Chinese cordyceps, a complex of bat moth larvae with *Ophiocordyceps sinensis* (*O. sinensis*), is well known as one of three great treasures of Chinese medicine, together with ginseng and deer antlers. Due to its medicinal and economic importance, wild resources are overexploited, resulting in a shortage of domestic and foreign supplies, so artificial cultivation of *Chinese cordyceps* is urgently needed. It is mainly distributed in alpine meadows at an altitude of 3000–5000 m on the Qinghai-Tibet Plateau where climate conditions are complicated and severe [1]. Its growth usually suffers from various environmental factors, especially in temperature, humidity and light. Thus, simulating the ecological growth environment of *Chinese Cordyceps* is crucial for its artificial cultivation [2, 3]. Variable temperature and low light have been reported to induce primordium formation [4, 5].*Chinese cordyceps* are expected to win for approximately 150 d, During this process, the water in the soil is in the form of crystalline water, so the *Chinese cordyceps* are subjected to water stress. The next spring, when the snow melts, this coercion disappears [6]. In addition, in our previous research, the colony of the fruiting body exhibited shrinkage and dry-cracking. Therefore, whether water stress can cause morphological transformation of the primordium or even stimulate its production is unclear.

Water is essential for the growth of microorganisms, and only free water is effectively available to microorganisms [7, 8]. Adequate water and humidity are necessary for the primordium growth of *Chinese cordyceps*. Water activity (a_w) is considered as a reliable index for measuring the actual utilization of water by fungi [8]. In *Eurotium cristatum*, different combinations of water activity and temperature had significant effects on mycelial growth and colony morphology, and the impact of water activity was more obvious [6, 7]. Moreover, the proportion of soluble sugars, amino acids and tea polyphenols in fermentation broth significantly differed during the biotransformation of tea with *Eurotium cristatum* [9]. Liu et al. reported that temperature and water activity were the most important factors affecting the mildew of stored corn [10]. Therefore, what is the mechanism of *O. sinensis* resistance to environmental stimuli under water stress?

As an organism evolves to cope with adversity, it gradually adopts a series of defensive strategies. The first strategy is osmotic regulation, such as the accumulation of malondialdehyde, polyphenols, betaine, free proline, and other small molecules [11]. The second strategy is to mobilize key ion transport proteins and channels to regulate ion homeostasis [12].The third strategy, antioxidant defense system activation, which mainly involves antioxidant enzymes and nonenzymatic antioxidants, initiates to remove excessive reactive oxygen species (ROS) [13]. Moreover, many manganese-responsive genes, such as spalt-like transcription factor 3 (*Sall3*), basic leucine zipper (*bZIP*), water stress tolerance zinc finger (*STZ*) and other signal-related protein kinases, have been identified [14]. In addition, several pathways involved in water stress, such as the MAPK pathway [15, 16], Ca^{2+}-dependent CDPK signaling pathway [17] and Ca^{2+}-dependent SOS signaling pathway [18], have been reported. It has been reported that adequate moisture and humidity are necessary for the growth of cordyceps ascospores [15], but how does Cordyceps resist environmental stimuli under water stress?

With the rapid development of high-throughput sequencing technology, RNA-seq has been widely considered to be an effective tool for exploring the molecular mechanism of adverse stress in organisms [19]. To date, a limited number of studies on the transcriptome of *Chinese cordyceps* have been published. Zhao et al. conducted a macro-transcriptomic study on the developmental period of wild *Chinese cordyceps* on the Tibetan Plateau and reported that although the microbial community composition differed among samples, trichoderma spp were present in all samples [20]. Zhong et al. used transcriptomic techniques to analyze the differences among the asexual mycelia, stiffeners and zygotes of *Chinese cordyceps*, and 391 genes were expressed in all three groups of samples. Compared with those in the asexual stage, 3049 genes were expressed in the sexual stage [21]. Li et al. used RNA-seq to analyze the transcripts of different periods and reported that the gene expression profiles at the progenitor formation and zygotic development stages were more similar than those at the mycelium stage, and the expression of mating type genes was highest at fertile sites [22]. However, gene expression changes in *O. sinensis* in response to water stress, as determined by RNA-seq, havn't been reported.

Metabolomics has the distinct advantage of providing a visual and dynamic representation of cellular physiological and biochemical processes. The relationships between metabolites and organismal representations can be more accurately represented [23]. At present, only a few metabolomics studies have been reported that extensively focused on comparing the chemical composition of wild and cultivated *Chinese cordyceps*. Four significantly variable metabolites were identified by nontargeted metabolomics, namely lysine, threonine, serine and arginine, while the nucleoside, nucleotide and adenosine contents were almost identical in the two materials [14]. Chen et al. used LC-MS to systematically study the metabolomes of wild Cordyceps and cultivated Chrysalis, and the results showed that Cordyceps contained high levels of amino acids, unsaturated fatty acids, peptides, glycosides and adenosine succinate [24]. However,

the metabolites involved in the response of *O. sinensis* to water stress are still unknown.

Adequate moisture is necessary for the growth of *Chinese cordyceps*. It is essential to understand the metabolic changes, transcriptional regulation, and physiological responses of bioactive and signaling compounds when exposed to water stress. In this study, the single-spore isolate TZ8-1 was used as the material, and the growth and development of *O. sinensis* under water stress were simulated by adding 3.8% NaCl to the medium. RNA-seq and metabolomics analyses were conducted to identify crucial water stress response genes and metabolites in *O. sinensis* under water stress, metabolomic and transcriptome analyses were combined to identify crucial pathways and related differentially expressed genes (DEGs) and metabolites (DEMs) involved in response to water stress. These findings will help to elucidate the effect of water stress on the growth and development of *Chinese cordyceps*.

Methods

Material

In 2019, the *O. sinensis* strain TZ8-1 was isolated from wild Chinese cordyceps via the formation of monocyst spores in Tianzhu County, Wuwei City, Gansu Province. It stored at the Institute of Biological Seedling Research, Lanzhou Jiaotong University. A 9 mm diameter single spore strain was transferred into the milk medium and incubated in a dark incubator at 18 °C for 45 d. Then, the materials were divided into five groups with 3 mL of 0.27 g/mL NaCl solution as a water stress treatment group for 30 d (Y30 group), 20 d (Y20 group), 10 d (Y10 group), 5 d (Y5 group) and 0 d (control). Samples from each group were collected and placed in lyophilization tubes at -80 °C. Three biological replicates were taken for each transcription group, and six biological replicates were taken for each metabolism group.

Observation of colony and mycelium morphology

Changes in the morphology and diameter of the strain colonies were observed regularly. *O. sinensis* colonies were lightly taped with adhesive tape and applied to slides. After the air bubbles were removed, the difference between the normal culture and water stress conditions was observed and recorded with a 100× light microscope.

Determination of the fresh weight and dry weight of colonies

The whole culture medium was removed, and the mixture was put into hot water at 60 °C. The agar was melted to obtain the complete strain colony, after which the colony surface water was removed with filter paper, and the fresh weight was measured. Afterward, the colonies were dried in a drying oven at 45 °C until constant weight, and 3 parallel experiments were performed for each group.

Determination of polysaccharide, mannitol, urea and betaine contents

The polysaccharide content was determined by the anthrone sulfate method [25], the mannitol content was determined by the sodium periodate colorimetric method [26], and the urea content was determined by the PDAB method [23]. The betaine content was determined by redwood salt colorimetry [27]. Three parallel tests were set up for each group.

Transcriptome sequencing process

Total RNA extraction and quality control were performed by Shanghai Ouyi Biomedical Technology Co. The library construction and sequencing work was performed by Shanghai Ouyi Biomedical Technology Co. The libraries were quality-checked with an Agilent 2100 Bioanalyzer and then sequenced with an Illumina HiSeq X Ten sequencer after passing the quality control of the constructed libraries. Then, 150 bp double-end data were generated. The raw fastq format sequence data were generated via throughput sequencing and quality filtered using Trimmomatic [28] software to obtain high-quality clean reads. The quality of the raw reads was filtered to obtain high-quality clean reads, which was followed by the use of Trinity (version 2.4) software. The transcript sequences were obtained by splicing the clean reads via paired-end splicing, and the longest sequences were then stitched according to their length and similarity.

Data analysis after sequencing

Unigenes were annotated to the NR, KOG, SwissProt, GO and KEGG [29] databases for data analysis using BLASTX with a threshold of e<1e-5 [30]. The expression of the unigenes was calculated using Bowtie2 software [31]. The number of unigene reads in each sample was obtained by eXpress [32] software, and then the data were normalized using the estimSizeFactors function in DESeq R package software [30]. The nbinomTest function was used to calculate the p value and fold change values. Differentially expressed unigenes with p-values<0.05 and FC values>2 were selected, and GO and KEGG enrichment analyses were performed on the differentially expressed unigenes to determine the biological functions and pathways in which the differentially expressed unigenes were mainly enriched. Unsupervised hierarchical clustering of the differentially expressed unigenes was performed to visualize the expression patterns of the differentially expressed unigenes among the different samples via heatmaps.

Weighted gene coexpression network analysis

The R package was applied to construct gene coexpression networks (WGCNA) based on the above transcriptome data (Zeng, et al., 2023). The RNA-seq data were normalized according to the criteria (log^2 (1+FPKM) values and soft threshold=12), and then the adjacency matrix was selectively generated on the basis of the scale-free topology criterion. The data were further converted to a topological overlapping matrix (TOM). Hierarchical clustering of genes was performed according to their differences, the hierarchical clustering tree was segmented with a dynamic tree- cutting algorithm, and the Pearson correlation algorithm was used to calculate the correlation coefficient and p-value between characteristic genes and the traits of the modules. An absolute correlation coefficient greater than or equal to 0.3 and p value less than 0.05 were used as the threshold values, and the modules related to each trait were screened. Scatter plots were drawn according to the correlation between module gene expression and module eigenene expression. TBtools (https://cloud.oebiotech.cn/) was used to visualize coexpression networks.

Metabolome sequencing process

The sample extraction and tests were performed by Shanghai Luminous Biotechnology Co. Chromatography analysis was performed according to the method described by He et al. with some changes [5]. A Dionex Ultimate 3000 RS UHPLC instrument fitted with a Q Exactive plus quadrupole-Orbitrap mass spectrometer equipped with a heated electrospray ionization (ESI) source (Thermo Fisher Scientific, Waltham, MA, USA) was used for metabolic profiling in both ESI-positive and ESI-negative ion modes. An ACQUITY UPLC HSS T3 column (1.8 μm, 2.1×100 mm) was used in both positive and negative modes. The binary gradient elution system consisted of (A) water (containing 0.1% formic acid, v/v) and (B) acetonitrile (containing 0.1% formic acid, v/v), and separation was achieved using the following gradient: 0 min, 5% B; 2 min, 5% B; 4 min, 25% B; 8 min, 50% B; 10 min, 80% B; 14 min, 100% B; 15 min, 100% B; 15 min, 5% and 16 min, 5% B. The flow rate was 0.35 mL/min, and the column temperature was 45 °C. All the samples were kept at 4 °C during the analysis. The mass range was from 100 to 1,000 m/z. The resolution was set at 70,000 for the full MS scans and 17,500 for the HCD MS/MS scans. The collision energy was set at 10, 20 and 40 eV. The mass spectrometer was operated as follows: spray voltage, 3,800 V (+) and 3,000 V (–); sheath gas flow rate, 35 arbitrary units; auxiliary gas flow rate, 8 arbitrary units; capillary temperature, 320 °C; aux gas heater temperature, 350 °C; and S-lens RF level, 50. The QCs were injected at regular intervals throughout the analytical run to provide a set of data from which repeatability could be assessed. Mass spectra were transformed using ProteoWizard software, and compounds were identified using The Human Metabolome Database (HMDB), Lipidmaps (v2.3), and METLIN databases. Differentially abundant metabolites with $P<0.05$ and variable importance in projection (VIP)>1 were subsequently screened. Finally, the KEGG database was used for differentially abundant metabolite enrichment and analysis.

qRT–PCR validation of differentially expressed genes

To verify the reliability of the transcriptome sequencing data, seven genes were selected for real-time PCR validation, and the 18 S rRNA gene was chosen as the internal reference gene. The primers for the internal reference gene and the target gene were designed using Roche software, and the primer list is detailed in Table S1.

Results

Effects of water stress on the mycelial morphology and physiological indicator accumulation of *O. sinensis*

Water stress significantly affected the growth of *O. sinensis* colonies in a time-dependent manner (Fig. 1). After exposure to water stress for different durations (0, 5, 10, 20, and 30 d), colony growth gradually decreased (Fig. 1a-e). In addition, differences in the mycelial morphology of *O. sinensis* under different treatment periods of water stress were more obvious. As shown in Fig. 1f-j, with increasing water stress duration, the conidia gradually disappeared, and the mycelial density increased, and the conidia became more twisted and arranged in network. Under 20 d of water stress, the dry weight, fresh weight and diameter of colonies of *O. sinensis* all reached significant levels, decreasing by 25.01%, 39.18% and 28.97%, respectively, compared to those of the control group (Fig. 1k-n). More interestingly, white hyaline mycelia and brown pigments appeared after 20 d-water stress (Fig. 1d-e). This may be related to changes in membrane permeability and lipid composition. To further explore the accumulation of cellular metabolites caused by water stress, three representative metabolites, urea, betaine, and polysaccharide, were measured. As shown in Fig S1, the urea, betaine and polysaccharide contents in *O. sinensis* in the presence of 5d water stress increased by 20.45%, 26.66%, and 11.43%, respectively. Subsequently, both the urea and polysaccharide contents tended to decrease, while the betaine content tended to increase. Changes in these substances might play important roles in response to water stress.

Analysis of relevant metabolite differences in *O. sinensis* under water stress

The results of quality control analysis and ion flow color map of the metabolomic data showed the stability of the mass spectrum system was good (S2.Fig). Prior to

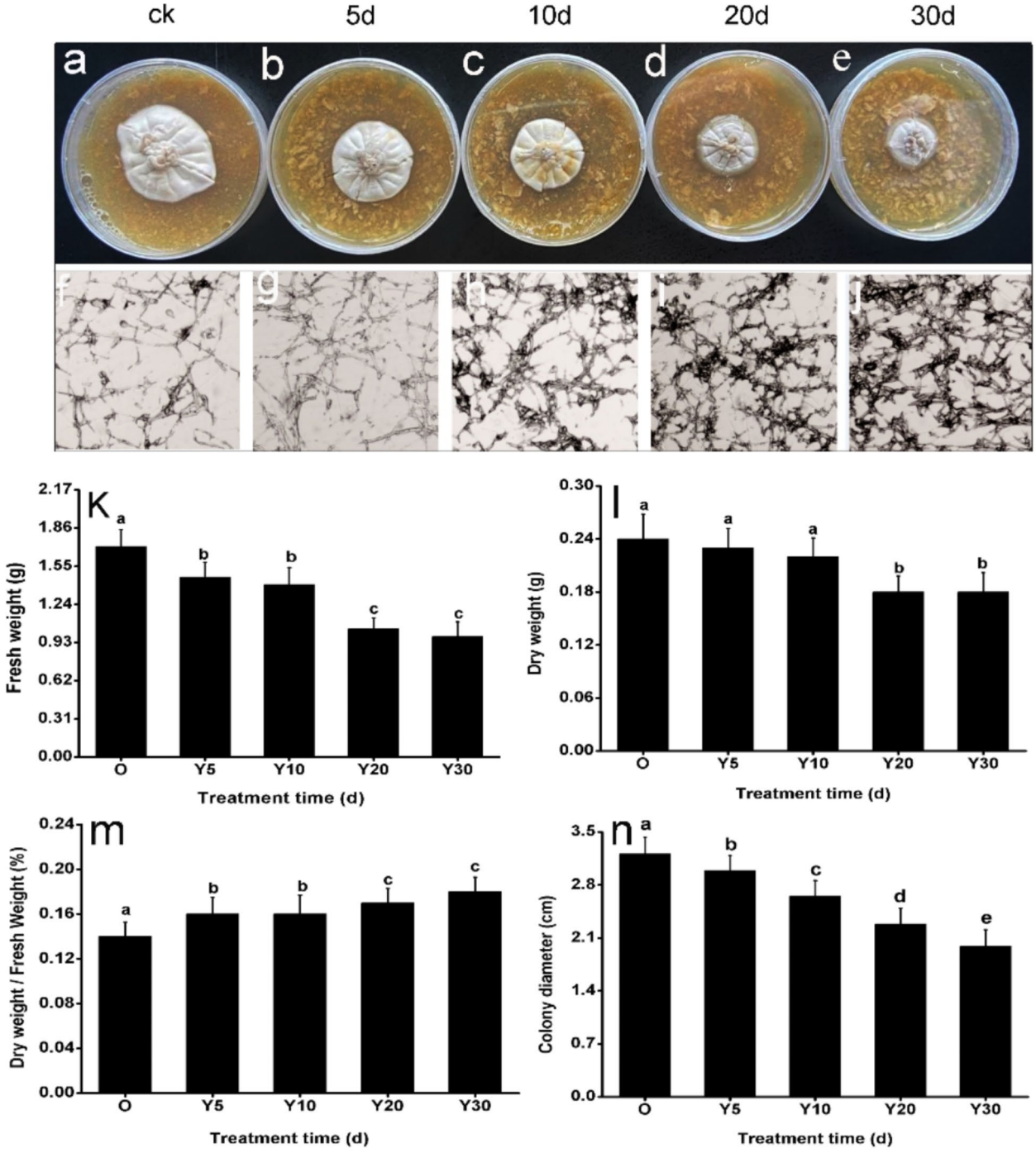

Fig. 1 The colony morphology (**a**-**e**), mycelial morphology (**f**-**j**) and growth indicators (**k**-**n**) of *O. sinensis* in different periods(ck,0d,5d,10d,20d,30d) under water stress

identifying the differentially abundant metabolites, PCA and OPLS-DA were conducted to distinguish the overall differences in metabolic profiles between the two groups. The PCA results showed that the separation trend was obvious between two sample groups (Fig. 2a). There were clear differences between two groups, and the samples within the groups were well reproducible. The OPLS-DA results showed that $Q^2=0.996$ and that the *p*-values were far less than 0.05, indicating model has the excellent predictive ability (Fig. 2b). The differentially accumulated metabolites (DAMs) in CK and Y20 groups were screened using the combination of the VIP value of the first principal component of the OPLS-DA model > 1 and the *p*-value of the t-test < 0.05. The clustering heatmap

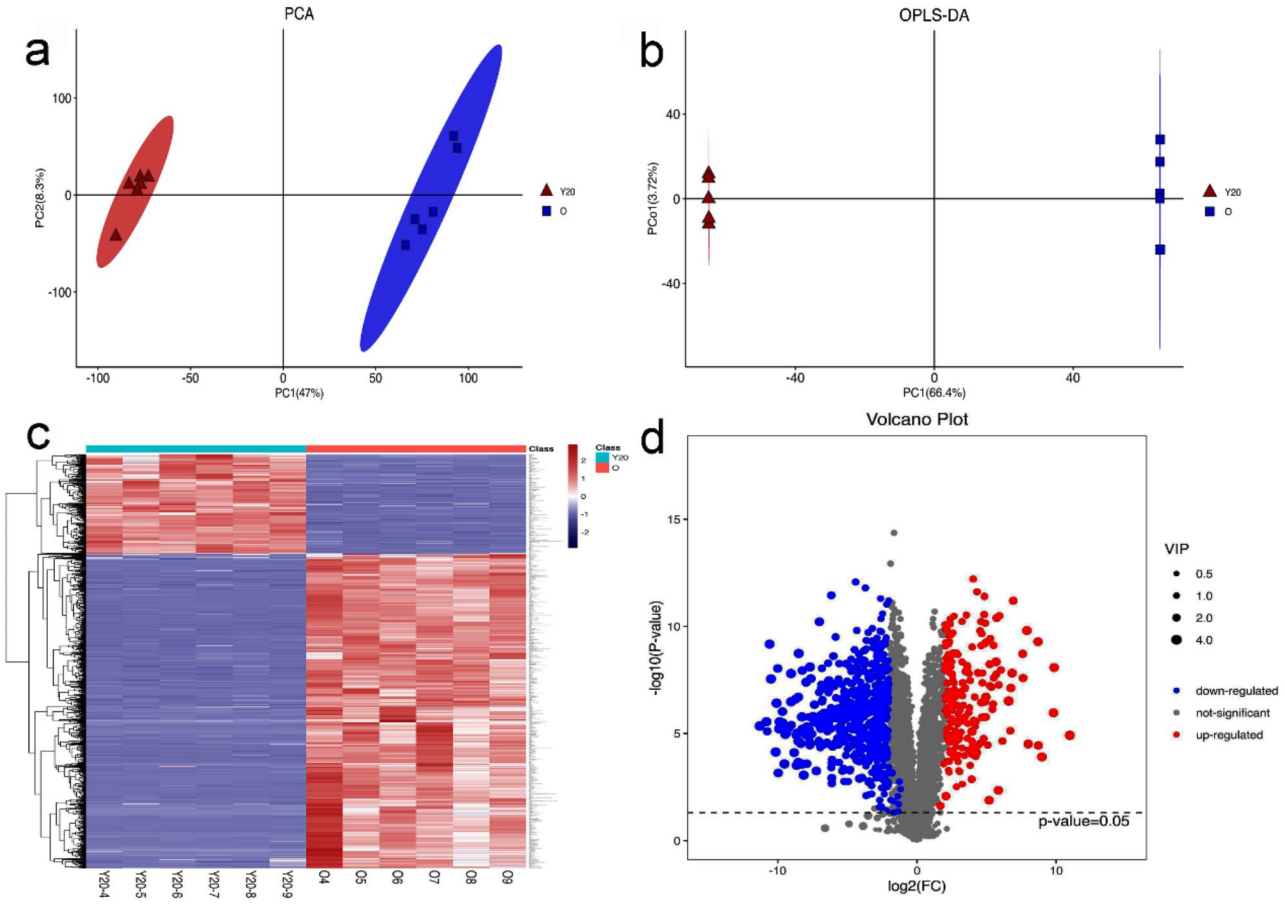

Fig. 2 (**a**) Principal component analysis (PCA) score plot. (**b**) Orthogonal partial least squares discriminant analysis (OPLS-DA) score plot. (**c**) Hierarchical clustering heat map of differential metabolites. (**d**) Volcano plot of differential metabolites

clearly demonstrated differentially abundant metabolites between CK and Y20 groups (Fig. 2c). A total of 5139 metabolites were detected in the volcano plot (Fig. 2d), of which 930 (706 upregulated and 224 downregulated) were significantly differentially abundant (Table S2). We inferred these 930 DEMs might be crucial metabolites of *O. sinensis* in response to 20 d-water stress.

Primary and secondary metabolites such as lipids, sugars, amino acids and active ingredients were indispensable for the response to various adverse conditions in fungi [33, 34]. To further uncover the differentially accumulated metabolites (DEMs) associated with water stress, hierarchical clustering was used to select crucial DEMs. Based on the criteria of a $|\log_2$ fold change$|>1$ and p-value<0.05, 107 metabolites were highly significantly differentially expressed and were classified into five categories. The group with the greatest accumulation was 50 lipid intermediates, among which palmitoyl CoA, undecanoic acid, 3-dehydroxycarnitine, and succinylcarnitine markedly accumulated, and other intermediates contents obviously decreased (Fig. 3a). The second group included 18 carbohydrate intermediates, except for 5-hydroxy-6-methoxyindole glucuronide, paromomycin, salicin, 4-(2-amino-3-hydroxyphenyl)-2, and 4-dioxobutanoic acid, were highly enriched, and the remaining intermediates tended to decrease (Fig. 3b). The third group included 15 amino acids, 4 of which included spermidine, L-aspartic acid, L-methionine, and L-cystathionine (Fig. 3c). In addition, 12 nucleic acids were up or down-regulated (Fig. 3d). Interestingly, 12 active components were detected, during which curcumin, spermine, cinnavalininate and DL-DOPA significantly accumulated after exposure to 20 d-water stress (Fig. 3e). These metabolites were further enriched in differentially abundant metabolite pathways mapped to the KEGG database in *O. sinensis*. As shown in S3.Fig, these DEMs were primarily accumulated in linoleic acid, α-Linolenic acid, arachidonic acid, carbohydrate and other metabolic pathways, indicating these DEMs in their metabolic pathways might play crucial roles when exposed to water stress in *O. sinensis*.

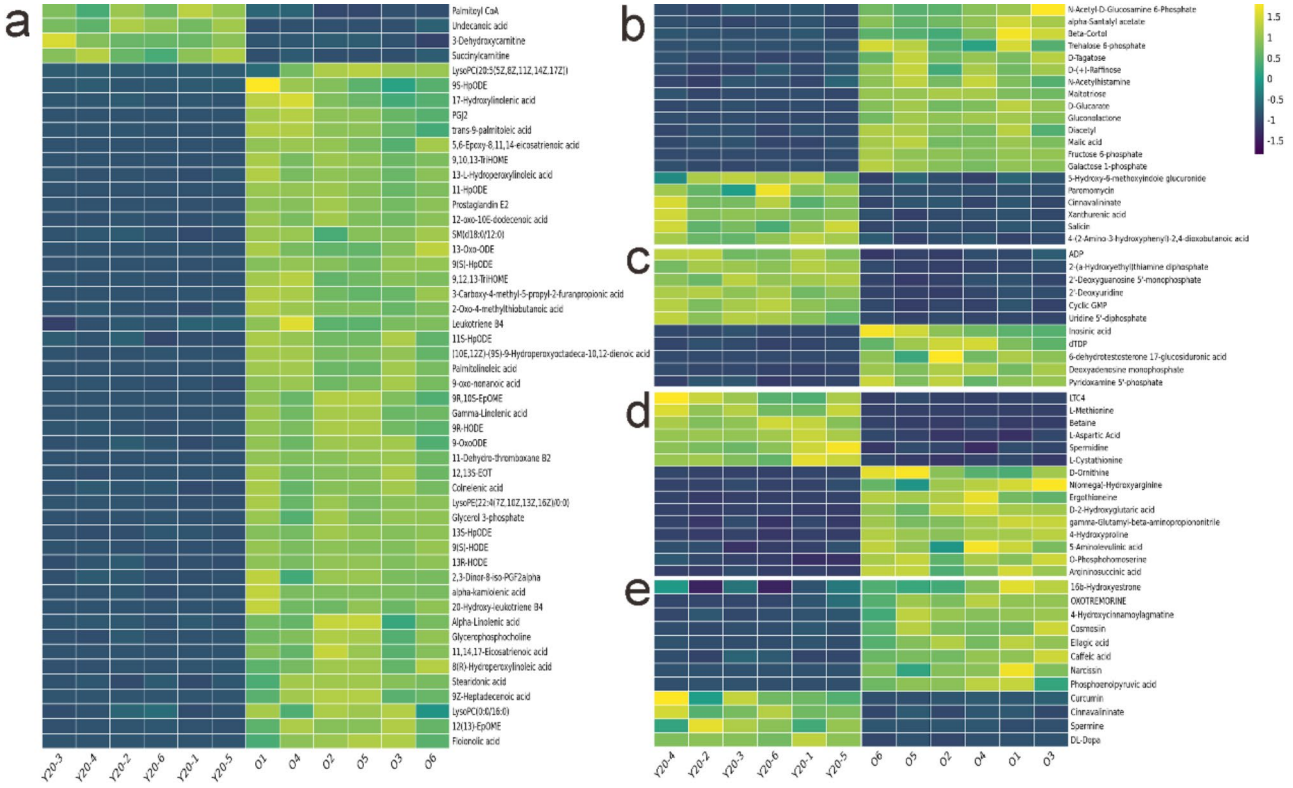

Fig. 3 Heatmap of different type DAMs metabolites exposed to water stress with TBtools software. (**a**) Amino acid. (**b**) Lipid metabolism. (**c**) Carbohydrate metabolism. (**d**) Nucleic acid metabolism. (**e**) Neurotransmitter, active factor. DAMs are selected based on VIP > 1 and $p < 0.05$

Transcriptome analyses of Chinese cordyceps in response to water stress

In this analysis, transcriptome sequencing of 15 samples was completed, and a total of 88.99 Gb of clean data was obtained. The effective data volume of each sample ranged from 6.01 to 6.97 G, and the distribution of Q30 bases ranged from 93.79 to 94.17%, with an average GC content of 59.67% (Table S3). The results of the PCA plot (S3. Fig) of three replicates of each group of samples clustered together, indicating good stability of the method and high data quality. With or without exposure to water stress, more than 3000 genes in each compared group were identified to be differentially expressed (Fig. 4a), indicating that these genes were regulated by the genetic background of the plants. Venn diagrams showed that a large number of DEGs were differentially expressed under water stress (Fig. 4b), indicating these DEGs might be induced by water stress. We further detected DEGs at four water stress exposure stages via functional enrichment analysis. As shown in Fig. 4c, most of upregulated or downregulated DEGs, such as those related to "catalytic activity" (GO: 0003824), "transporter activity" (GO: 0003824), and "membrane", were enriched in fungal stress responsed in Y20 vs. CK comparison group (GO: 0016491). The KEGG analysis results showed these DEGs were involved in primary and secondary metabolic pathways, such as "carbohydrate metabolism", "amino acid metabolism" and betaine metabolism (S4. Fig). These specific DEGs might play important roles in response to water stress.

Gene coexpression analysis after exposure to water stress by WGCNA

To elucidate the regulatory network of the successive water stress stages of *O. sinensis*, 15 samples containing 12,924 genes were subjected to WGCNA. After filtering out genes with low fluctuation in expression (standard deviation ≤ 0.5), 5585 genes (median absolute deviation, MAD > 0.25) were screened out to establish a directed network. We chose a power of β = 12 based on the scale-free topology criterion to generate a hierarchical clustering tree (Fig. 5a). Nine coexpression modules were identified with mergeCutHeight = 0.25 (marked with different colors, Fig. 5b), during which genes number in each module ranged from 56 to 1159. A total of 701 genes that didn't attributed to any modules were classified into the gray module.

Then, the correlations between the modules' eigengenes and stages were explored (Fig. 5b). The module trait relationship results showed that the darkmagenta ($r = 0.99$, $p = 2e\text{-}12$; $r = -0.28$, $p = 0.3$) and darkorange ($r = 0.55$, $p = 0.03$; $r = -0.58$, $p = 0.2$) modules were gradually

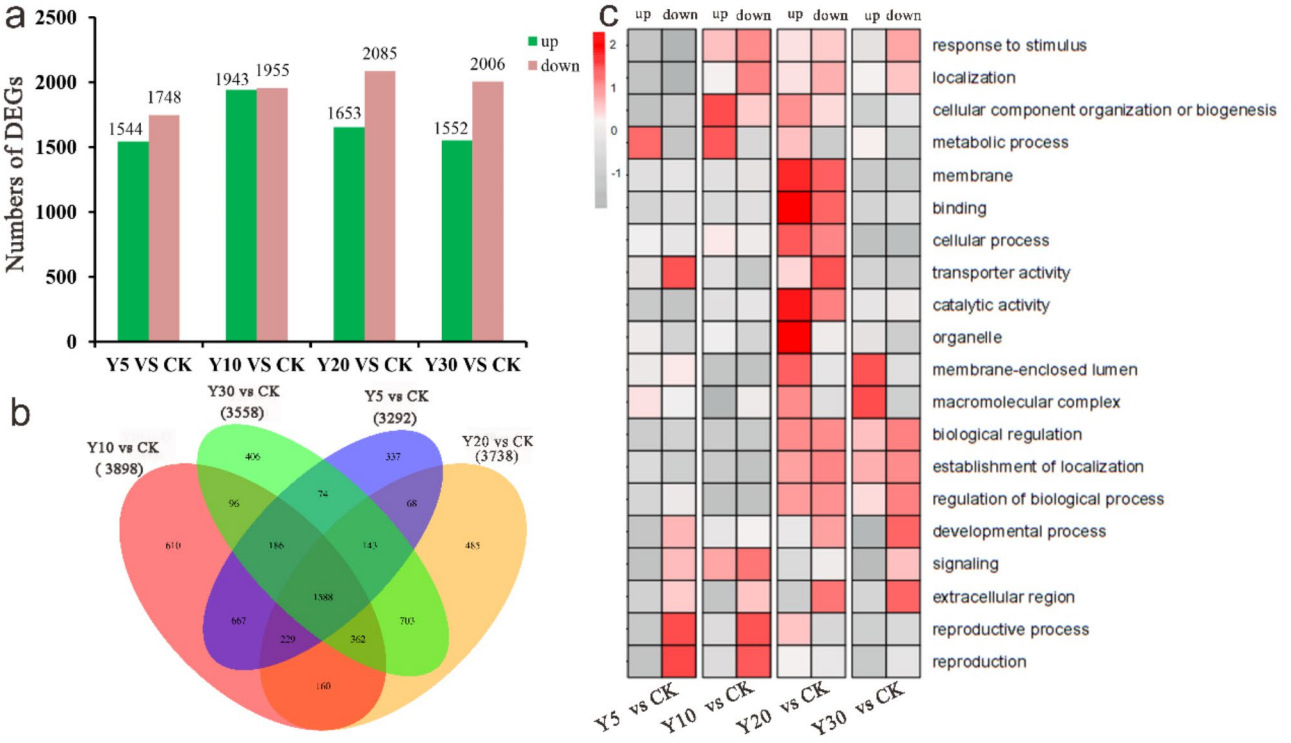

Fig. 4 Differentially expressed genes responding to different periods under water stress. (**a**) DEG distribution between different periods analyzed. The number of genes differentially expressed is indicated on the top of the histograms. (**b**) Venn diagrams comparing shared DEGs exposed to water stress (**c**) Enriched gene ontology (GO) terms of down- and up-regulated genes responding to water stress at different periods.(corrected p-value was normalized) with TBtools software

negatively correlated, while the genes in the darkolivegreen module (r =-0.49, p=0.07; r=0.7, p=0.003) showed the opposite pattern when exposed to successive water stress. Notably, the bisque4 module with 316 genes was strongly correlated with the Y20 vs. CK comparison group (r=0.88, p=4e-0.5), implying these genes might strongly response to 20d-water stress.

Characteristics and hub genes of the transcriptional regulatory modules correlated with 20-d water stress

The significant correlations between the gene expression of 20d-water stress and module membership (MM) in bisque4 were shown in Fig. 6a. Based on the GO annotation analysis, 32 prominent GO terms (corrected p<0.05) were identified, the top three of which were "oxidoreductase activity" (GO: 0016491, corrected p value=5.72E-14), "extracellular region" (GO: 0005576, corrected p value=2.07E-11) and "plasma membrane" (GO: 0005886, corrected p value=1.63E-08) (Fig. 6b, Table S5). KEGG enrichment analysis revealed these 316 DEGs were closely correlated with betalain biosynthesis, tyrosine metabolism, linoleic acid metabolism, fructose and mannose metabolism and starch and sucrose metabolism (Fig. 6c). We further explored hub genes in these pathways (Fig. 6d). In betalain biosynthesis pathway, the L-DOPA synthesis-related gene *TYR* (LOC127822312) was markedly upregulated, while the L-DOPA decomposition-related genes *COMT* (LOC127895355) and *DODA* (LOC312300) were generally downregulated in plants exposed to water stress. For tyrosine metabolism, two hub genes, *HPD* (LOC127625417) and *TYR* (LOC127822312), were closely related to the biosynthesis of eumelanin and homogentisate. Another hub gene (HGD) was markedly downregulated under water stress. Overall, we hypothesized that the synthesis of betalain and eumelanin might be closely correlated with the water stress resistance of *O. sinensis.* EC:1.13.11.62 (fatty acid oxygenase) and EC:3.1.1.4 (cytosolic phospholipase A2) were directly related to linoleic acid metabolism for the accumulation of linoleic acid (Fig. 6e), indicating these hub genes and biological pathways might play indispensable roles in the response to water stress in *O. sinensis*. Additionally, three hub genes, *SOU1*, *mtlD*, and *PFK*, were highly upregulated, but *SORD* and *LRA2* were downregulated in fructose and mannose metabolism. Moreover, 6 hub genes, *sacA*, *EGLC*, E3.2.1.58 (glucan 1,3-beta-glucosidase), *otsA*, *PYG* and *otsB*, were closely associated with starch and sucrose metabolism (Fig. 6e), indicating these hub genes and carbohydrate metabolism pathways contributed to resistance of water stress.

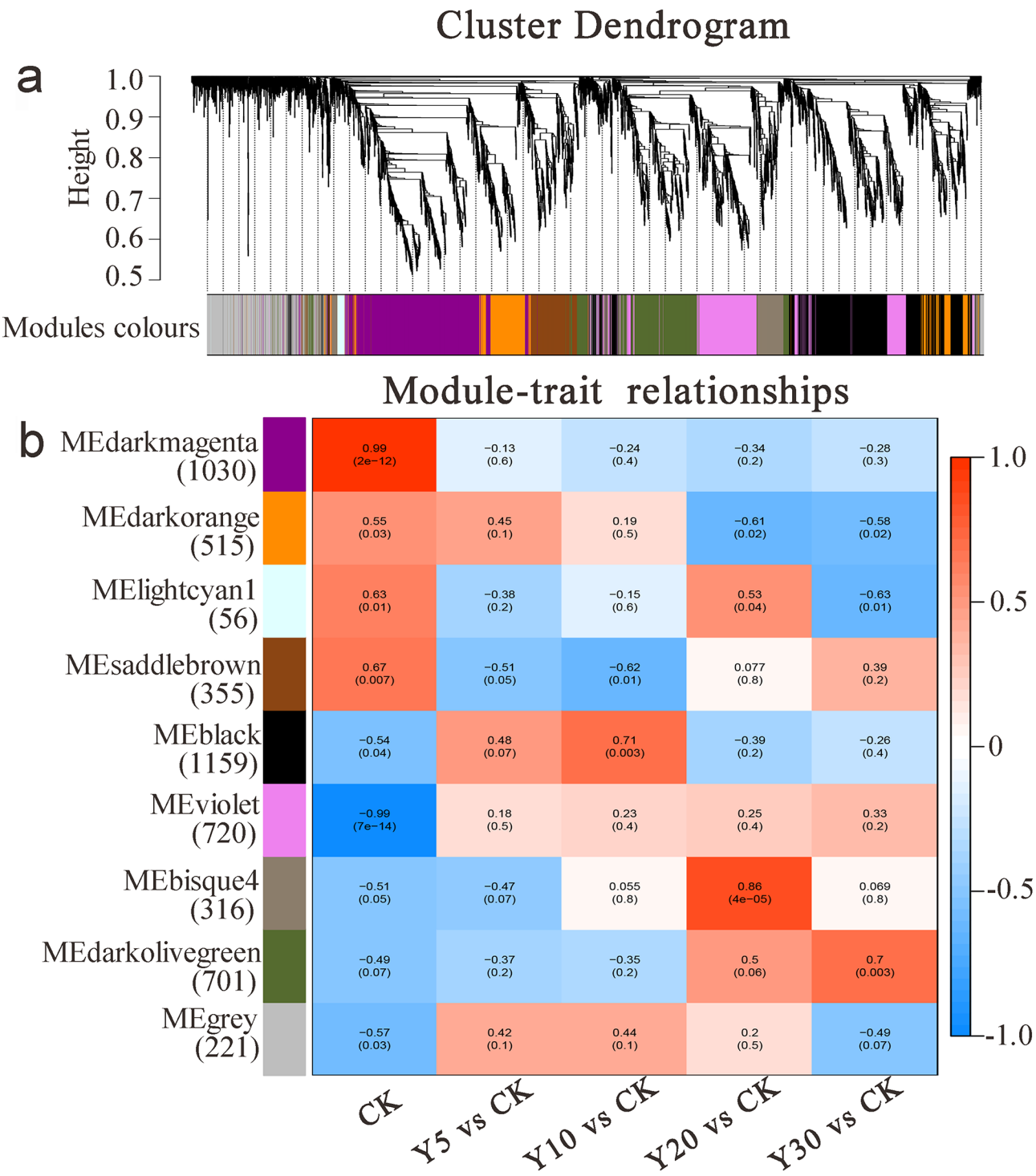

Fig. 5 WGCNA of the transcripts in *O. sinensis*. (**a**) The gene clustering tree is constructed by dissTOM matrix with weighted correlation coefficients. The lower part of the figure is divided into the distribution of genes of each module. The same color represents the same module. The color of Dynamic TreeCut is the module identified by dynamicTreeCut method. (**b**). Correlations between modules eigengenes and stages. The color of each module is the same as that in (**a**)

Candidate genes and metabolites related to betalain biosynthesis and tyrosine metabolism under stress

Based on the results of the combined metabolome and transcriptome analysis, the metabolic pathway of tyrosine and betalain in *O. sinensis* was constructed (Fig. 7). In tyrosine metabolic pathway, three genes related to pigment production, tyrosinase (*TYR*), aspartate aminotransferase (*GOT1*), and 4-hydroxyphenylpyruvate

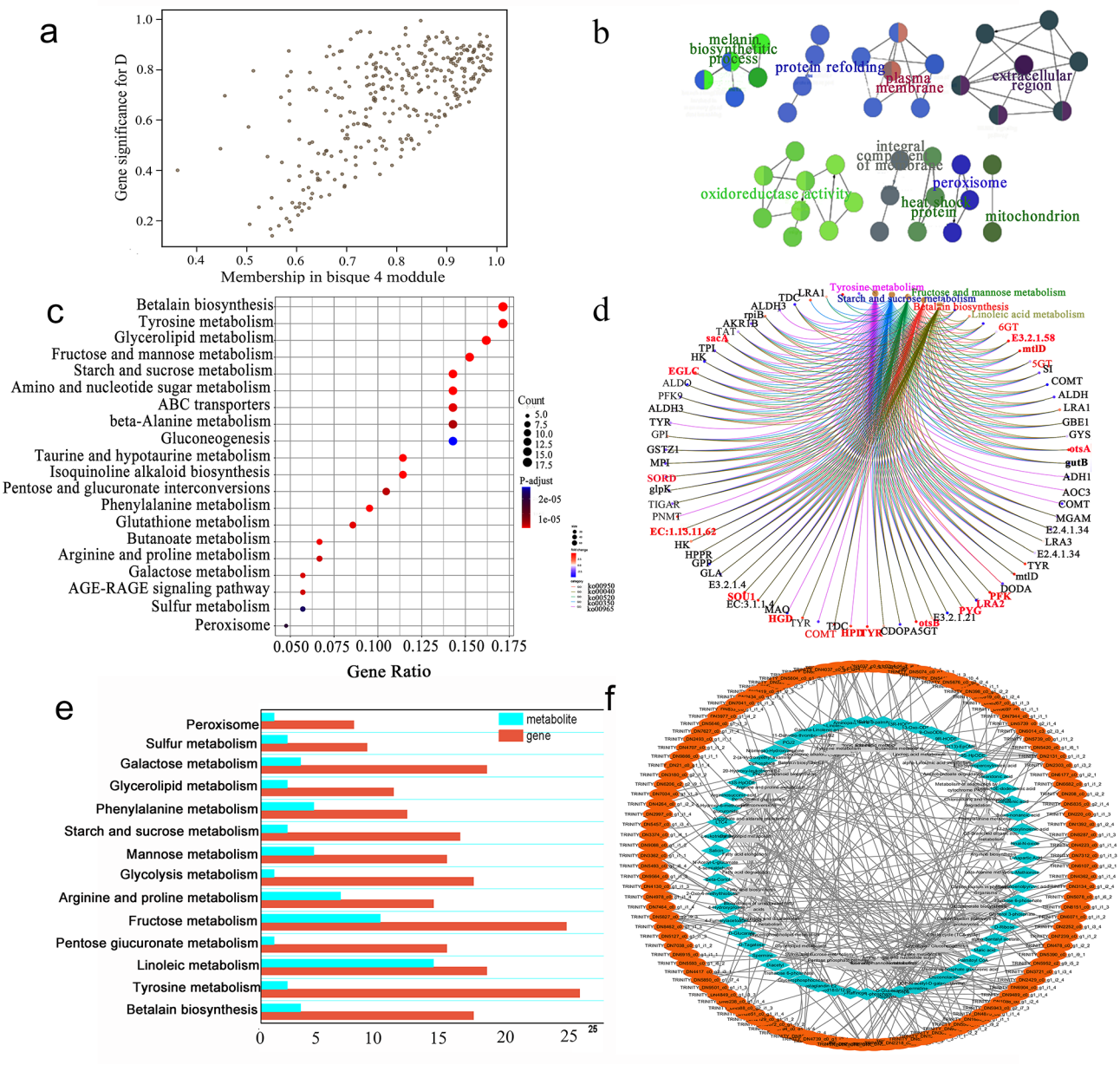

Fig. 6 Expression profile and transcriptional regulatory network in the bisque4 modules. (**a**) Catterplots of gene significance versus module membership for the bisque4. (**b**) GO analysis of genes in the bisque4 module. Each circle represents an enrichment category, and the size of the circle indicates the number of genes. (**c**) KEGG analysis of genes in the bisque4 module (top 20) with p-value < 0.05. (**d**) Co-expression network of the hub genes and its enriched pathways in the bisque4 modules with circular_cnetplot. (**e**) Integrated analyses of the transcriptome and metabolome of the KEGG pathways related to fatty acid, carbohydrate metabolism and betalain biosynthesis exposed to salt stress. The yellow line indicates a p value of 0.01, representing a very significant difference, and the blue line; The p value is 0.05, which represents a significant difference of gene; The purple pink line indicates a p value of 0.01, representing a very significant difference, and the green line; The p value is 0.05, which represents a significant difference of metabolite. (**f**) Correlation network of DEGs and DAMs involved in fatty acid, carbohydrate metabolism and betalain biosynthesis (**b**). Peacock blue diamond represent metabolites, orange ellipse indicate genes and gray triangle represents metabolic pathways. Grey straight line and curve represent represent positive and negative correlations, respectively, conducted by a Pearson's correlation coefficient > 0.8 or < − 0.8 (q-value < 0.1), respectively

dioxygenase (*hppD*), were upregulated, while homogentisate 1,2-dioxygenase (*hmgA*) was downregulated. Moreover, metabolomics analysis revealed that the contents of L-beta-(3,4-dihydroxyphenyl)alanine (L-DOPA), eumelanin and homogentisate significantly increased and that of acetoacetate markedly decreased. In addition, betanin, a key osmotic substance in betanin biosynthesis, was found to be highly accumulated in plants exposed to water stress due to the upregulation of betanidin 5-O-glucosyltransferase(*5GT*) and cyclo-DOPA 5-O-glucosyltransferase (*CPODA- 5GT*).

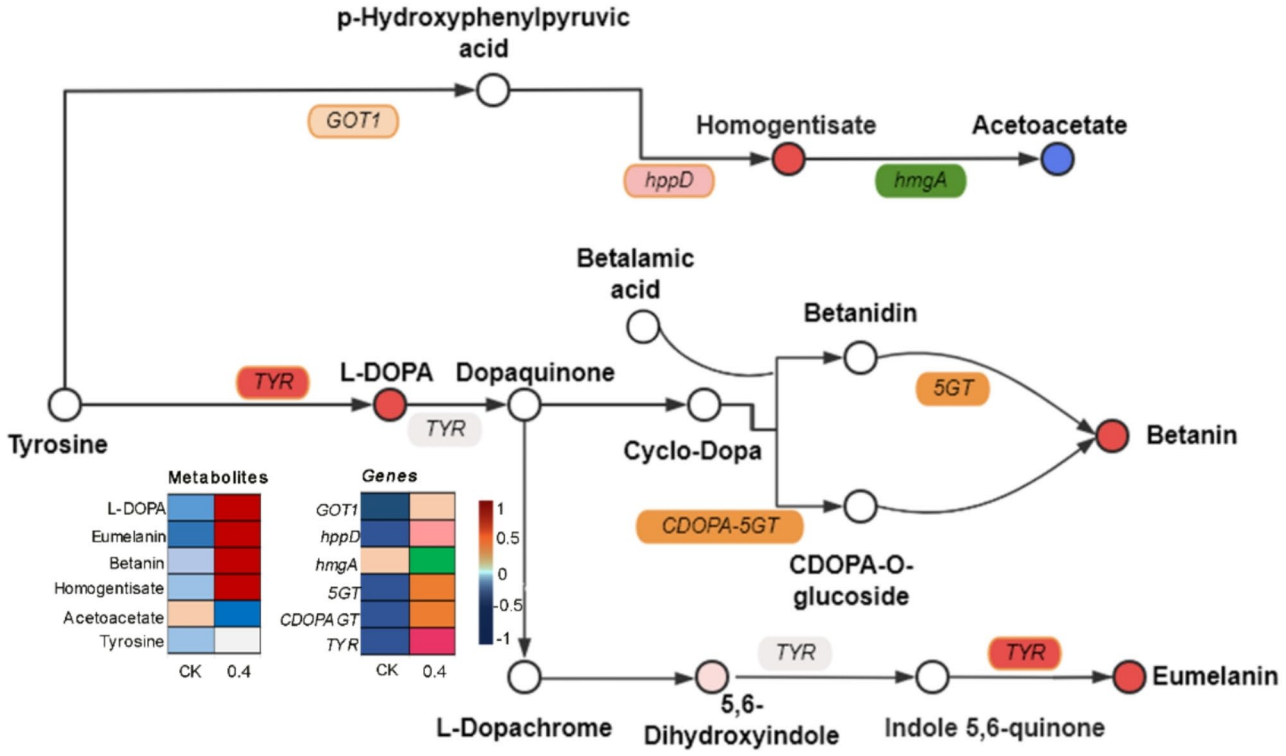

Fig. 7 The differentially expressed genes (DEGs) and differentially expressed metabolites (DEMs) involved in betalain biosynthesis and tyrosine metabolism in *O. sinensis* in response to salt stress. The circles represent the metabolites regulated exposed to salt stress (red indicates up-regulation; blue indicates down-regulation). The oblongs represent the genes regulated exposed to salt stress (red indicates up-regulation; blue indicates down-regulation)

Overall, the tyrosine and betanin metabolic pathways might be closely related to the water stress tolerance mechanism of *O. sinensis* through enhancing cell osmotic potential and producing antioxidant pigments.

Candidate genes related to carbohydrate metabolism and fatty acid degradation under water stress

On the basis of the combined metabolome and transcriptome analysis, the metabolic pathways of carbohydrates, the TCA cycle and fatty acid degradation in *O. sinensis* were identified (Fig. 8), and several candidate genes were significantly differentially expressed after exposure to water stress for 20 d. In the carbohydrate metabolic pathway, 4 genes related to polysaccharides, sucrose-6-phosphate hydrolase (*sacA*), endo-1,3−1,4-beta-glycanase (*EGLC*), trehalose-6-phosphate synthase (*otsA*) and trehalose-phosphatase (*otsB*), were significantly upregulated, while galactosidase alpha (*GLA*) and UDP-glucose pyrophosphorylase 2 (*UGP2*) were downregulated. Notably, key intermediates, such as β-D-fructose-6P, D-fructose-6P, and tagatose, had almost no accumulation. In the fatty acid degradation pathway, a key gene, 2,3-dehydroadipyl-CoA hydratase (*paaF*), was found to be highly expressed in each step of fatty acid degradation, but there was little accumulation of degraded intermediates. Interestingly, the accumulation of acetyl-CoA was also significantly reduced. Furthermore, in the tricarboxylic acid cycle, succinate dehydrogenase flavoprotein subunit (*SDH1*) and fumarate hydratase (*fumB*) are highly expressed, and metabolomics analysis revealed that the levels of succinyl-CoA and malate were significantly decreased. The above results indicated that carbohydrate metabolism and fatty acid degradation might be the most important ways to provide a large amount of acetyl-CoA for the TCA cycle to generate a large amount of energy for organisms when exposed to water stress.

Discussion

Relationship between water stress and cordyceps primordium development

Under wild conditions, mycelium will grow from the cracks in the head of the rigor next spring after the zombie winters, and the mycelium will twist to form a dense mycelium mass and then form primordia, which will continue to develop into fruiting bodies. In this process, temperature, water stress or the "nutrient-poor" state of the grassland in winter may stimulate *Chinese cordyceps* to shift from vegetative growth signals to reproductive growth or the result of a combination of signals. We also observed a similar situation; when *Chinese cordyceps* was cultured on artificial media with fruiting bodies after 300 d of culture, most of the media exhibited a shrinking,

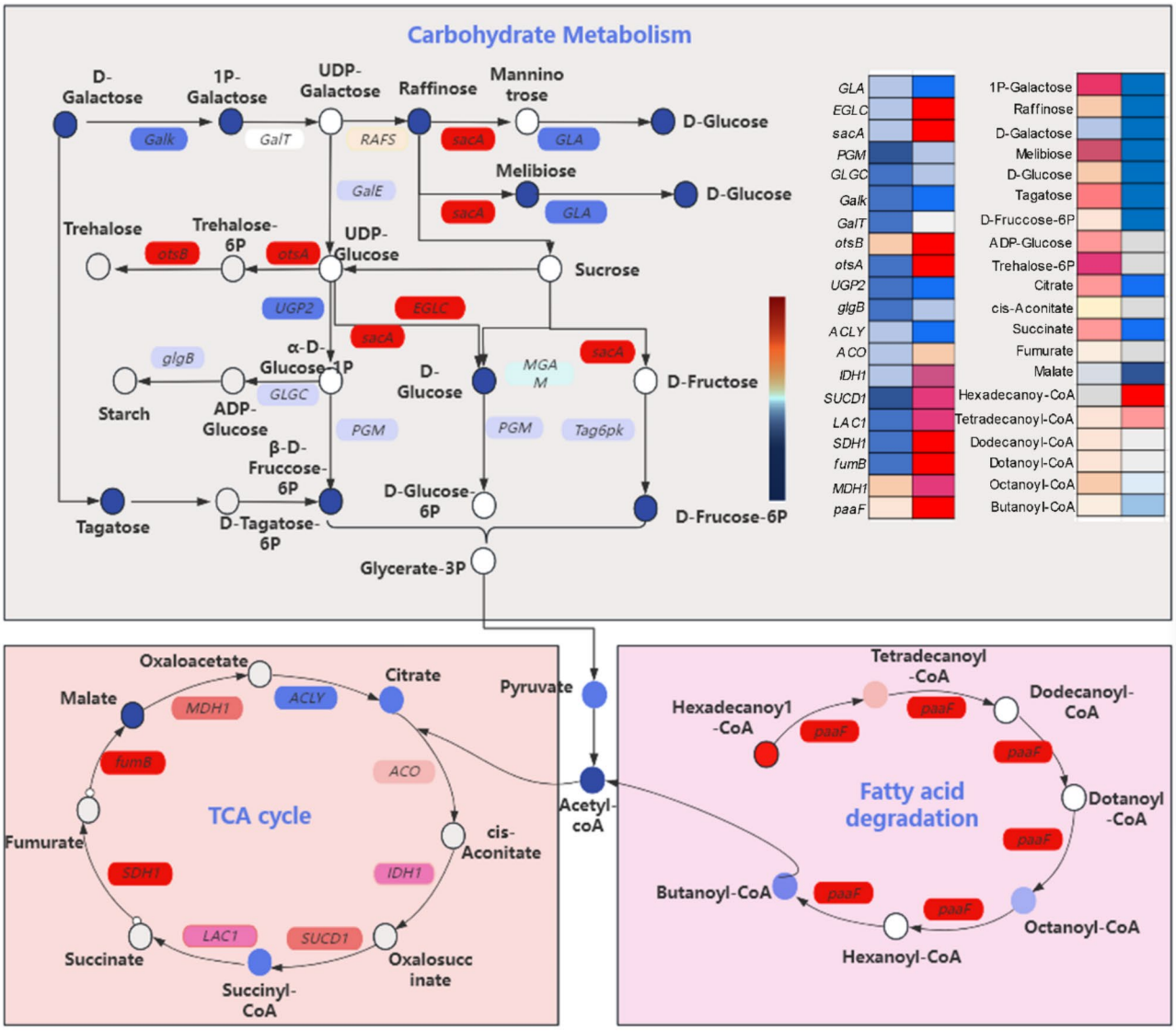

Fig. 8 The differentially expressed genes (DEGs) and differentially expressed metabolites (DEMs) involved in carbohydrate metabolism and fatty acid degradation in *O. sinensis* in response to salt stress. The grey box represents the carbohydrate metabolism, the orange box represents TCA cycle, the pink box represents fatty acid degradation. The circles represent the metabolites regulated exposed to salt stress (red indicates up-regulation; blue indicates down-regulation). The oblongs represent the genes regulated exposed to salt stress (red indicates up-regulation; blue indicates down-regulation)

cracking phenomenon, and a "poor nutrition" state. The formation of fungal fruiting bodies was a complicated dynamic process. In general, mycelial aggregation and kinking mark the differentiation and development of the primordium. During the formation of fruity bodies of *Lentinus edodes*, the initial mycelia locally gather and knot under nutrient stress, and the knot density gradually increases to form dense mycelial clusters, which eventually develop into the primary base [35]. However, if the bisporus were subjected to moderate water stress in the early stage of mushroom formation (during soil covering) and at the end of the term, it would help to enhance the root development of the mushroom [36]. Similarly, in our study, water stress caused a large number of mycelial kinks and changed mycelial morphology (Fig. 1), which may stimulate the formation of Cordyceps primordia. Research on the mechanism of changes in this growth stage was the basis for the industrialization of artificial cultivation of *Chinese cordyceps*.

The role of betalain biosynthesis and the tyrosine metabolism pathway under stress

Some metabolites, such as polysaccharides, mannitol, and betaine, have been widely proven to be the core factors involved in fungal defense against osmotic stress. In fungi, organisms can produce and accumulate mannitol under osmotic stress to improve osmotic pressure tolerance [37]. Compared with that in different growth stages,

the mannitol content in *Chinese cordyceps* reached a maximum before the primordium matured [38]. Similarly, our results also showed that mannitol content peaked at Y5 and then continuously decreased. On the one hand, we speculated that the early accumulation of mannitol may be related to its increase in cell osmotic potential and subsequent gradual decrease because the body needs to degrade mannitol to replenish other essential compounds. On the other hand, mannitol may not be the main osmoregulator of *O. sinensis* subjected to water stress. Under water stress, betaine rapidly accumulated in organisms to maintain the osmotic balance inside and outside cells to maintain the normal physiological function of cells [39]. Rathinasabopathi et al. reported that the biosynthesis of betaine in *Pichia pastoris* mainly depended on choline oxidase (*CMO*) and betaine aldehyde dehydrogenase (*BADH*). When *CMO* and *BADH* were coexpressed in *P. pastoris* GS115, the glycine betaine content in the recombinant yeasts was 28- to 35-fold greater than that in the control group, which was more resistant to water stress [40], indicating that betaine played a crucial role in the response to water stress. Similarly, betaine tended to increase continuously in our study. To adapt to adverse conditions, *Chinese cordyceps* increased its L-DOPA content by altering tyrosinase activity (Fig. 7). On the one hand, L-DOPA can accumulate in large quantities in cells as an amino acid and improve cell osmotic potential; on the other hand, L-DOPA is the precursor of betaine, a very important osmoregulatory substance in the long-term adaptation process of *Cordyceps cordyceps* [41]. With the accumulation of betaine and amino acids, mycelia gradually expand. More importantly, betaine can participate in fat metabolism by supplying methyl groups, and choline can form water-soluble lecithin with fatty acids and phosphoric acid to participate in fat movement [42]. The newly grown mycelium of *Chinese cordyceps* was white and transparent, and we inferred that this change may be related to changes in the lipid composition of the membrane, resulting in changes in the permeability of the cell membrane. This hypothesis was further confirmed by our results. There were 14, 7 and 4 DEMs annotated in the linoleic acid, α-linolenic acid and arachidonic acid metabolic pathways, respectively. These pathways were the most significant pathways in the KEGG pathway annotation, and all of them were related to phosphatidylcholine (PC) (Fig. 1). S3), one of the most important components of membrane lipids on cell membranes [43], indicating that water stress significantly affects the cell membrane of *Chinese cordyceps*. In addition, the kinking and reticular arrangement of mycelia (Fig. 2) facilitated transmembrane transport of substances and signal transduction and increased resistance to adversity [44].

The role of carbohydrate metabolism and the fatty acid degradation pathway under stress

Carbohydrate metabolism and fatty acid degradation are essential for nutrient and energy availability in *O. sinensis* plants exposed to water stress. In the present study, 1P-galactose, raffinose, D-glucose, melibiose, tagatose, and D-fructose-6P markedly decreased in the presence of 20 d-water stress. D-Galactose and tagatose were converted into β-D-fructose-6P, UDP-galactose and raffinose were converted into D-glucose-6P, and raffinose can also be converted into D-fructose-6P, and then converted to pyruvate. These genes were mainly positively regulated by *sacA*, *otsA*, *otsB*, and *EGLC*, especially *sacA*, and played pivotal roles in the metabolism of various sugars, which was consistent with previous research showing that *sacA* was the key regulatory gene in carbohydrate metabolism in *O. sinensis* [45]. The decrease in polysaccharide content may be because organisms need to speed up energy metabolism in response to water stress and continuously consume their own nutrients to maintain normal life activities. A similar energy supply pattern has been reported for other fungi [46]. We speculated that because the pyruvate produced only by the glycolysis pathway was insufficient to supply the capacity to initiate the TCA cycle under water stress, the β-oxidation pathway initiated to collaborate with the glycolysis pathway to increase capacity. It has been reported that the β-oxidation pathway is the crucial production pathway of fungi in response to adverse conditions [47]. This speculation was further confirmed, showing that there was nearly no accumulation of intermediate products related to the β-oxidation pathway of palmitic acid, which were obviously positively regulated by *paaF*. Interestingly, acetyl-CoA was also significantly reduced under 20d-water stress. Furthermore, we found that intermediate metabolites associated with the TCA cycle were also significantly reduced (Fig. 8), suggesting that a large amount of energy was consumed when subjected to water stress. Overall, it was likely that the glycolysis and β-oxidation pathways of the palmitic acid pathway worked together to produce large amounts of acetyl-CoA, which subsequently entered the tricarboxylic acid cycle (TCA) pathway to produce large amounts of ATP in *O. sinensis* exposed to water stress.

Conclusions

In this study, combined transcriptome and metabonomic analysis was conducted to reveal the mechanism of water stress tolerance in *O. sinensis*, and the results revealed metabolites and genes related to betalain biosynthesis and tyrosine, linoleic acid, fructose and mannose and starch and sucrose metabolism pathways, all of which played crucial roles in response to water stress. These metabolic pathways might work cooperatively to

generate enough acyl-CoA and then enter the TCA cycle to provide energy exposed to water stress. Moreover, the betalain biosynthesis and tyrosine metabolism pathway might contribute to water stress in *O. sinensis* by producing osmoregulatory substances (betaine) and antioxidant pigments (eumelanin). This study provides a theoretical basis for determining the relationship between the growth and water stress of *O. sinensis* and provides important information for further realizing the industrialization of artificial cultivation of *Chinese cordyceps*.

Supplementary Information

The online version contains supplementary material available at https://doi.org/10.1186/s12864-024-10785-2.

Supplementary Material 1

Supplementary Material 2

Supplementary Material 3

Supplementary Material 4

Supplementary Material 5

Supplementary Material 6

Acknowledgements

We gratefully acknowledge the financial support of the National Natural Science Foundation of China (Grant No. 31560003) and the Young Scholars Science Foundation of Lanzhou Jiaotong University (No. 2022020). Lanzhou Science and Technology Project (2022-2-51).The authors are grateful to all the reviewers for their valuable suggestions regarding the improvement of the manuscript.

Author contributions

Li He: Writing–original draft, Methodology, Investigation. Fang Xie: Visualization, Supervision. Zhao He Chen: Writing, review and editing, supervision, and conceptualization. Bo Zhou: Writing–review & editing, Formal analysis. Fan Xiao: Visualization, Validation, Conceptualization.

Funding

This work was funded by the National Natural Foundation of China, Regional Foundation (31560003) and Lanzhou Jiaotong University Youth Fund (2022020). Lanzhou Science and Technology Project (2022-2-51).

Data availability

Sequence data that support the findings of this study have been deposited in the National Center for Biotechnology Information (NCBI) database with the accession number PRJNA1098460.

Declarations

Ethics approval and consent to participate

Samplings were conducted on private land, we got permission from the land owner to collect materials.

Consent for publication

Not applicable.

Competing interests

The authors declare no competing interests.

Received: 17 April 2024 / Accepted: 9 September 2024
Published online: 29 October 2024

References

1. Martel J, Ko YF, Liau JC, Lee CS, Ojcius DM, Lai HC, Young JD. Myths and realities surrounding the mysterious caterpillar fungus. Trends Biotechnol. 2017;35(11):1017–21. https://doi.org/10.1016/j.tibtech.2017.06.011.
2. Lei W, Zhang G, Peng QY, Liu X. Development of *Chinese cordyceps* through plant-mediated interkingdom host colonization. Int J Mol Sci. 2015;16(8):17482–93. https://doi.org/10.3390/ijms160817482.
3. Li X, Wang F, Liu Q, Li QP, Qian ZM, Zhang ZL, et al. Developmental transcriptomics of *Chinese cordyceps* reveals gene regulatory network and expression profiles of sexual development-related genes. BMC Genomics. 2019;20(1):337. https://doi:10.1186/s 12864-019-5708-z.
4. Xie F, He L, Su QJ, Xia YX, Zhou G, Chen ZH. Transcriptome analysis the effects of light treatment on *Ophiocordyceps sinensis* metabolism. Int J Med Mushrooms. 2022;24(8):81–97. https://doi.org/10.1615/IntJMedMushrooms.2022044445.
5. He L, Xie F, Zhou G, Chen ZH, Wang JY, Wang CG. Transcriptome and metabonomics combined analysis revealed the energy supply mechanism involved in fruiting body initiation in *Chinese cordyceps*. Sci Rep. 2023;13:9500. https://doi.org/10.1038/s41598-023-36261-7.
6. He J. Harvest and trade of caterpillar mushroom *(Chinese cordyceps)* and the implications for sustainable use in the Tibet region of southwest China. J Ethnoph Armacol. 2018;221:8690. https://doi.org/10.1016/j.jep.2018.04.022.
7. Maneffa AJ, Stenner R, Matharu AS, Clark JH, Matubayasi N, Shimizu S. Water activity in liquid food systems: a molecular scale interpretation. Food Chem. 2017;237:1133–38. https://doi.org/10.1016/j.foodchem.2017.06.046.
8. Bremer E, Krämer R. Responses of microorganisms to osmotic stress. Annu Rev Microbiol. 2019;8(73):313–34. https://doi.org/10.1146/annurev-micro020518-115504.
9. Liu M, Gong Z, Liu H, Wang JH, Wang D, Yang YJ, Zhong S. Structural characterization and anti-tumor activity in vitro of a water-soluble polysaccharide from dark brick tea. Int J Biol Macromol. 2022;30(205):615–25. https://doi:10.1016/j. ijbiomac.2022.02.089.
10. Liu J, Qi M, Huang Y, Guo J, Zhang JC, Li C, et al. Effects of oils on feed mildew and quality. Anim Sci J. 2017;88(8):1075–81. https://doi.org/10.1111/asj12733.
11. Zhao C, Zhang H, Song C, Zhu JK, Shabala S. Mechanisms of plant responses and adaptation to soil salinity. Innov (Camb). 2020;1(1):100017. https://doi:10.10 16/j.xinn.2020.100017.
12. Ren ZH, Gao JP, Li LG, Cai XL, Huang W, Chao DY, et al. A rice quantitative trait locus for salt tolerance encodes a sodium transporter. Nat Genet. 2005;37:1141–46. https://doi.org/10.1038/ng1643.
13. Smeets K, Opdenakker K, Remans T, Sanden SV, Belleghem FV, Semane B et al. Cadmium responses in *Arabidopsis thaliana*: Glutathione metabolism and antioxidative defense system. J Plant Physiol. 2007;166(18):1982-92. https://doi.org/10.1016/j.jplph. 2009.06.014.
14. Zhao G, Zhao YY, Yu XL, Kiprotich F, Han H, GuanRZ, et al. Nitric oxide is required for melatonin-enhanced tolerance against salinity stress in rapeseed (brassica napus) Seedlings. Int J Mol Sci. 2018;19(7):1912. https://doi.org/10.3390/ijms19071912.
15. Mathien S, Tesnière C, Meloche S. Regulation of mitogen-activated protein kinase signaling pathways by the ubiquitin–proteasome system and its pharmacological potential. Pharmacol Rev. 2021;73(4):263–96. https://doi.org/10.1124/pharmrev.120.
16. Zhang M, Zhang SJ. Mitogen-activated protein kinase cascades in plant signaling. Integr Plant Biol. 2022;64(2):301–41. https://doi.org/10.1111/jipb.13215.
17. Li YJ, Fei XW, Dai HF, Li JY, Zhu WJ, Deng XD, et al. Genome-wide identification of calcium-dependent protein kinases in *chlamydomonas reinhardtii* and functional analyses in nitrogen deficiency-induced oil accumulation. Front Plant Sci. 2019;10:1147. https://doi.org/10.3389/fpls.2019.01147.
18. Rudnytska MV, Palladina TA. Effect of preparations methyure and Ivine on Ca^{2+}-ATPases activity in plasma and vacuolar membrane of corn seedling roots under water stress conditions. Ukr Biochem J. 2017;89(1):76–81. https://doi.org/10.15407/ubj89.
19. Amirbakhtiar N, Ahmad IA, Ghaffari MR, Firouzabadi FN, Shobbar Z. Transcriptome response of roots to water stress in a salinity-tolerant bread wheat cultivar. PLoS ONE. 2019;14:e0213305. https://doi.org/10.1371/journal.pone.0213305.
20. Zhang X, Liu Q, Zhou W, Li P, Alolga RN, Qi LW, Yin XJ. A comparative proteomic characterization and nutritional assessment of naturally and artificially cultivated *cordyceps Sinensis*. J Proteom. 2018;181:24–35. https://doi.org/10.1016/j.jprot.2018. 03.029.

21. Zhong X, Gu L, Wang HZ, Lian DH, Zheng YM, Zhou S, et al. Profile of *Ophiocordyceps Sinensis* transcriptome and differentially expressed genes in three different mycelia, sclerotium and fruiting body developmental stages. Fungal Biol. 2018;122(10):943–51. https://doi.org/10.1016/j.funbio.2018.05.011.
22. Li X, Wang F, Liu Q, Li QP, Qian ZM, Zhang XL, et al. Developmental transcriptomics of *Chinese cordyceps* reveals generegulatory network and expression profiles of sexual development-related genes. BMC Genomics. 2019;20(1):337. https://doi:10.1186/s 12864-019-5708-z.
23. Matich EK, Soria N, Aga DS, Atilla-Gokcumen GE. Applications of metabolomics in assessing ecological effects of emerging contaminants and pollutants on plants. J Hazard Mater. 2019;373:527–35. https://doi.org/10.1016/j.jhazmat.2019.02.084.
24. Chen L, Liu Y, Guo Q, Zheng Q, Zhang W. Metabolomic comparison between wild *Chinese cordyceps* and artificial cultured cordyceps militaris. Biomed Chromatogr. 2018;11:e4279. https://doi.org/10.1002/bmc.4279.
25. Jin LQ, Xu ZW, Zhang B, Yi M, Weng CY, Lin S, et al. Genome sequencing and analysis of fungus hirsutella sinensis isolated from *Chinese cordyceps*. AMB Express. 2020;10(1):105. https://doi.org/10.1186/s13568-020-01039-x.
26. Giannini G, Alekseeva A, Naggi A, Salvini L, Tei L, Santis RD. Characterization of therapeutic protein AvidinOX by an integrated analytical approach. Anal Bioanal Chem. 2018;410(2):553–64. https://doi.org/10.1007/s00216-017-0754-3.
27. Ratriyanto A, Mosenthin R. Osmoregulatory function of betaine in alleviating heat stress in poultry. J Anim Physiol Anim Nutr (Berl). 2018;102(6):1634–50. https://doi.org/10.1111/jpn.12990.
28. Bolger AM, Lohse M, Usadel B. Trimmomatic: a flexible trimmer for Illumina sequence data. Bioinformatics. 2014;30(15):2114–20. https://doi.org/10.1093/bioinformatics/btu170.
29. Yan WJ, Hussain H, Chung HH, Julaihi N, Tommy R. Transcriptome dataset of sago palm in peat soil. Data Brief. 2022;41:107908. https://doi:10.1016/j.dib.2022.
30. Buchfink B, Xie C, Huson DH. Fast and sensitive protein alignment using. Diam Nat Methods. 2015;12(1):59–60. https://doi.org/10.1038/nmeth.3176.
31. Wilton R, Szalay AS. Performance optimization in DNA short-read alignment. Bioin Formatics. 2022;38(8):2081–87. https://doi.org/10.1093/bioinformatics/btac06.
32. Roberts A, Pachter L. Streaming fragment assignment for real-time analysis of sequencing experiments. Nat Methods. 2013;10(1):71–3. https://.
33. Ranner JL, Schalk S, Martyniak C, Parniske M, Gutjahr C, Stark TD, Dawid C. Primary and secondary metabolites in *Lotus japonicus*. J Agric Food Chem. 2023;71(30):11277–303. https://doi.org/10.1021/acs.jafc.3c02709.
34. Zhang ZY, Meng JH, Zhang Q, Zhou H, Li GL. MM, Transcriptomic analysis of the orchestrated molecular mechanisms underlying fruiting body initiation in *Chinese cordyceps*. Gene.2020;https://doi.org/10.1016/j.gene.2020. 145061.
35. Ng WL, Ng TP, Kwan HS. Cloning and characterization of two hydrophobin genes differentially expressed during fruit body development in *Lentinula edodes*. FEMS Microbiol Lett. 2000;185(2):139–45. https://doi.org/10.1111/j.1574-6968.2000.tb09052.x.
36. Ji JT. Effects of water stress on dynamic development quality and water use efficiency of greenhouse mushroom. Trans Chin Soc Agricultural Eng. 2021;37(06):205–13. https://doi.org/10.11975/j.issn. 2021.06. 025.
37. Zahid N, Deppenmeier U. Role of mannitol dehydrogenases in osmoprotection of Gluconobacter oxydans. Appl Microbiol Biotechnol. 2016;100:9967–78. https://doi.org/10.1007/s00253-016-7680-8.
38. Chun YJ, Lu ZM, Luo ZS, Li SS, Li H, Geng Y, et al. Comparative analysis of cordyceps acid content in different growth stages of *Chinese cordyceps*. J Agric Food Chem. 2019;67(31):8476–84. https://doi.org/10.1021/acs.jafc.9b02705.
39. Fu JJ, Wang Y, Yang JH, Huang DQ, Zhang Q, Huang Y, et al. Mitigating the detrimental effects of water stress on anammox process: a comparison between glycine betaine and mannitol. Sci Total Environ. 2002;851(2):158221. https://.
40. Wang SH, Yao QH, Tao JM, Qiao YS, Zhang Z. Co-ordinate expression of glycine betaine synthesis genes linked by the FMDV 2A region in a single open reading frame in *Pichia pastoris*. Appl Microbiol Biotechnol. 2007;77(4):891–99. https://doi.org/10.1007/s00253-007-1222-3.
41. Breitel D, Brett P, Alseekh S, Fernie AR, Butelli E, Martin C. Metabolic engineering of tomato fruit enriched in L-DOPA. Metab Eng. 2021;65:185–96. https://doi.org/10.1016/j.ymben.2020.11.011.
42. Alloing G, Travers I, Sagot B, Rudulier DL, DuPont L. Proline betaine uptake in *Sinorhizobium meliloti*: characterization of Prb, an opp-like ABC transporter regulated by both proline betaine and salinity stress. J Bacteriol. 2006;188:6308–17. https://doi.org/10.1128/JB.00585-06.
43. Wiczew D, Szulc N, Tarek M. Molecular dynamics simulations of the effects of lipid oxidation on the permeability of cell membranes. Bioelectrochemistry. 2021;141:107869. https://doi.org/10.1016/j.bioelechem.2021.107869.
44. Riquelme M, Aguirre J, Bartnicki-García S, Braus GH, Feldbrügge M, Fleig U, et al. Fungal morphogenesis, from the polarized growth of hyphae to complex reproduction and infection structures. Microbiol Mol Biol Rev. 2018;82(2):e00068–17. https://doi.org/10.1128/MMBR.00068-17.
45. Lee EJ, Jang KH, Im SY, Lee YK, Farooq M, Farhoudi R, et al. Physico-chemical properties and cytotoxic potential of *Chinese cordyceps* metabolites. Nat Prod Res. 2014;29(5):455–59. https://doi.org/10.1080/14786419.2014.948438.
46. Lin S, Liu ZQ, Baker PJ, Yi M, Wu H, Xu F, et al. Enhancement of cordyceps polysaccharide production via biosynthetic pathway analysis in *Hirsutella Sinensis*. Int J Biol Macromol. 2016;92:872–80. https://doi.org/10.1016/j.ijbiomac.2016.08.002.
47. Zhang ZQ, Chen Q, Tan Y, Shuang S, Dai R, Jiang XH, et al. Combined transcriptome and metabolome analysis of alfalfa response to thrips infection. Genes (Basel). 2021;12(12):1967. https://doi.org/10.3390/genes12121967.

Publisher's note